Geometrical Issues in Design for Binder Jetting – The Effect of anisotropic dimensional Change on Sintering

M. Zago[1[0000-0002-2798-5482]], N.F.M. Lecis[2[0000-0003-3926-8189]], M. Vedani[2[0000-0003-3626-5732]], I. Cristofolini[1[0000-0003-2787-1271]]

[1] Department of Industrial Engineering, University of Trento, Via Sommarive 9, 38123, Trento - Italy.
[2] Department of Mechanical Engineering, Politecnico di Milano, Via Privata Giuseppe La Masa 1, 20156, Milan - Italy
marco.zago-1@unitn.it

Abstract. Recent research has been focused on the binder jetting (BJ) additive manufacturing technique due to the high potential possibilities in industrial applications. The actual limitation of BJ process can be attributed to the difficult control of the product quality. In fact, a high dimensional variation occurs on sintering, which can detrimentally affect dimensional and geometrical precision, when not properly considered in the design step.
This paper aims at investigating the influence of sintering on the dimensional change of through holes, with different diameter size and different axis orientation with respect to the building direction. Samples were measured in the green and sintered state by means of a coordinate measuring machine in order to calculate the diameter shrinkage. The empirical data were successfully compared with the prevision of an analytical model demonstrating that diameter shrinkage is influenced by: the anisotropic dimensional change, the axis orientation and the position of the two diametral opposite points used to identify the diameter. A deep analysis of the results showed a non-negligible effect of the gravity-induced load and of the inhomogeneous shrinkage on sample geometry. This study highlighted that the analytical model may serve as a basis in the design step for improving the dimensional quality of BJ product.

Keywords: Binder Jetting, Design for Additive Manufacturing, Dimensional and Geometrical Precision.

1 Introduction

Binder jetting additive manufacturing technique has currently demonstrated promising results due to the high production rate and low manufacturing cost [1]. Even though the performance of BJ product might be lower in comparison to laser powder bed fusion product, BJ can theoretically process any type of metal and ceramic materials, and it does not require controlled atmosphere, neither high energy heat source in the printing machine [2]. The BJ working flow is split in two fundamental operations: the printing operation and the sintering process. The printing step consists in spreading a layer of

powder on a working plate, then injecting a binder agent in correspondence of the section of the CAD file of the product. After layer-by-layer shaping, the green part is obtained. However, metal powders are weakly bonded, therefore the green part is cured, to partially enhance the mechanical resistance, aiming at safely handling the product in the further operation. The residual powders of the printing operation are then carefully removed from the green part. Finally, part is debinded and sintered in order to obtain the final product.

The successful development of BJ and other AM technologies needs for specifically oriented design methods and guidelines, known as Design for Additive Manufacturing (DfAM) [3, 4]. Since the great advantage of the AM is the free form design approach, large part of research has been focused on the shape, investigating both topology optimization [5] and geometrical product specification [6, 7].

The assessment and control of the geometrical quality of AM parts are fundamental for the standardization of the manufacturing process, and particularly in BJ, because the sintering operation can detrimentally affect the dimensional and geometrical precision of sintered-based product [8]. For this reason, the effect of sintering process has to be considered in the design step. A few studies experimentally measured the anisotropic dimensional change on sintering [9–11]. Kafara et al. studied the influence of binder quantity on the dimensional accuracy and mechanical strength [12]. Islam et al. focused on the dimensional accuracy of as-built BJ cylinders [13]. Ollison and Berisso investigated the cylindricity of green parts with different axis orientation with respect to the fabrication direction [14]. However, the influence of the anisotropic dimensional change on sintering on the quality of sintered BJ products is not specifically investigated in depth in the scientific literature.

In previous works the anisotropic dimensional change on sintering and the effect on the dimensional precision have been investigated in depth [15–17]. This work aims at investigating the influence of sintering on dimensional variation of through holes with different diameter size and different orientation. An analytical model was derived, aimed at predicting the dimensional change of diameters. The results were successfully compared with the experimental measurements.

2 Method & Model

In the section 2.1, the dimensions and geometrical characteristic of samples are reported, in addition to the material and experimental procedure adopted. Section 2.2 concerns the statement of the assumptions and the analytical formulation of the model for the prediction of diameter shrinkage.

2.1 Experimental procedure

Five samples were fabricated in order to study the dimensional precision of cylindrical holes. Each sample has four through holes equally spaced in a plane of 20x70 millimeters, which is inclined at angles of 0°, 30°, 45°, 60° and 90° with respect to the fabrication direction as shown in Fig. 1. The dimensions of such plane and the diameter of the holes were kept constant in all of the samples. The other sample dimensions were

optimized in order to yield the depth of the hole in a range close to 10 millimeters, to directly compare the measurements results.

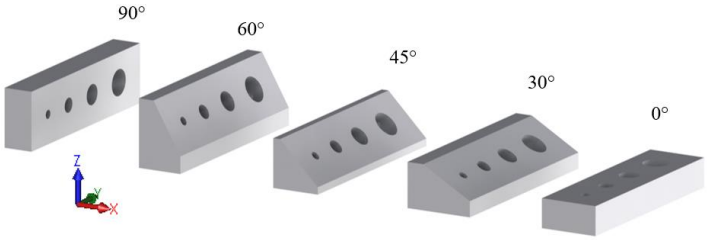

Fig. 1. Nominal geometry and name of the 5 samples.

The nominal dimensions of the five samples are reported in Table 1, referring to dimensions shown in Fig. 2.

Table 1. Nominal dimensions of the linear dimensions and the cylindrical holes of the five geometries (all dimensions are in millimeters).

	0°	30°	45°	60°	90°
LX1	20	23.19	16.62	15.41	10
LX2	-	5.87	2.47	5.41	-
LY1	70	70	70	70	70
LZ1	10	15.41	16.62	23.19	20
LZ2	-	5.41	2.47	5.87	-
W	-	20	20	20	-
ϕ_3	3	3	3	3	3
ϕ_5	5	5	5	5	5
ϕ_7	7	7	7	7	7
ϕ_9	9	9	9	9	9
$H_{\phi 3}$	10	11.15	12	11.15	10
$H_{\phi 5}$	10	10.58	11	10.58	10
$H_{\phi 7}$	10	10	10	10	10
$H_{\phi 9}$	10	9.42	9	9.42	10

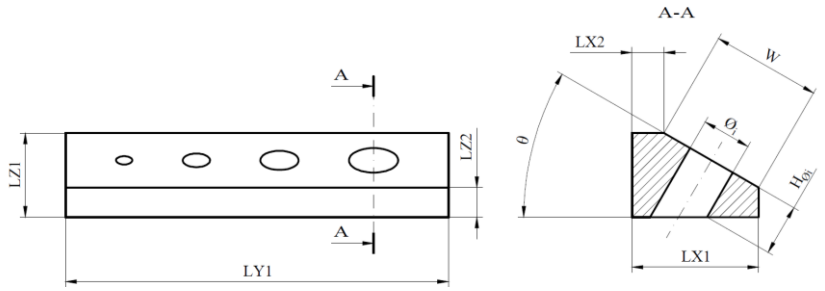

Fig. 2. Section view and conventional name of the main features in inclined samples.

The samples were fabricated by an ExOne Innovent+ printing machine, set-up parameters are reported in Table 2. Gas atomized AISI 316L powder was used, being one

of the most promising material currently studied in scientific literature and applied in industrial production [18].

Table 2. BJ process parameters.

Layer thickness	Saturation level	Recoat	Roller	Ultrasonic intensity
50 μm	55%	90 mm/s	500 rpm	100%

All samples were printed, cured and sintered in a single batch in order to minimize the variability of the manufacturing process. The larger dimension of all the samples was set parallel to the printhead movement direction, so that the variability of the fabrication process would affect all the samples in the same way. In this work it is assumed that the sample location does not affect the dimensional and geometrical precision, despite some variability was observed by Vitolo et al [19].

After the printing operation, samples were cured at 180°C for 180 minutes and successively samples were extracted by the printing chamber and extra powders were removed.

The measurement of the green samples was performed with a Hexagon DEA Global Image 07-07-07 coordinate measuring machine. The CMM mounted a Renishaw SP600M touch-probe which has a maximum permissible error of 1.5 + L/333 μm in touch acquisition mode according to ISO 10360-2 [20]. The diameter of the tip used is 1 mm and the effective working length of the stylus is 20.5 mm, to guarantee the inspection of the holes through all the depth, also considering the shrinkage on sintering.

In the set-up of the measurement procedure, the sample was carefully blocked to the CMM working plane as shown in Fig. 3. The clamping system allowed accessing all the planes and holes, also limiting the shadow effect of the supports.

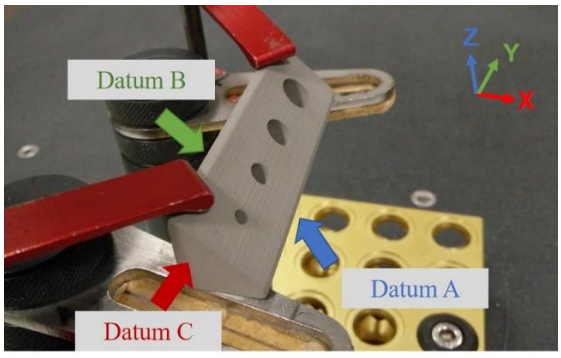

Fig. 3. Example of the clamping system adopted for the measurement of green and sintered samples and the planes used as datum reference.

A direct-computer-control measurement routine was developed for each sample. A 3-2-1 alignment procedure was initially performed to define the three datum planes. The primary datum plane (A) was identified on the bottom plane, which corresponds to the

first plane fabricated by the layer-by-layer construction. The secondary datum plane (B) corresponds to the plane parallel to YZ plane, and the third datum plane (C) to the plane parallel to XZ plane, as shown in the Fig. 3.

A pattern of 50 to 150 points was acquired on each plane to maximize the measurement data points for the reconstruction of the plane by a gaussian best fit least squares method. The linear dimensions of samples were derived as distances between planes. Moreover, the effective depth of the hole ($H_{\phi i}$, where i subscript refers to the different nominal diameters, as in Table 1) can be computed by the trigonometric relationships expressed by equation (1) for samples 30° and 45°, and equation (2) for sample 60°. The effective depth corresponds to the depth which includes a complete cylinder, as displayed in Fig. 2.

$$H_{\phi i} = \frac{LZ1}{\cos\theta} - \left(\frac{\phi_i}{2} + \frac{W}{2}\right) tan\,\theta \tag{1}$$

$$H_{\phi i} = \frac{LX1}{\sin\theta} - \left(\frac{\phi_i}{2} + \frac{W}{2}\right) cot\,\theta \tag{2}$$

On the basis of the effective depth of the holes, the circular section of the cylinder was measured at five equidistant levels, as shown in Fig. 4a. On each level, 12 points were acquired on the circular section, 30° spaced, according to the reference system shown in Fig. 4b.

Consequently, on each circular section six values of the diameter can be calculated by equation (3), as the distance of the diametral opposite points, where x_j, y_j, z_j are the coordinates of each point, subscript j referring to values from 1 to 6, and subscript i to the nominal diameter.

$$\phi_{i-j} = \sqrt{\left[\left(x_j - x_{j+6}\right)^2 + \left(y_j - y_{j+6}\right)^2 + \left(z_j - z_{j+6}\right)^2\right]} \tag{3}$$

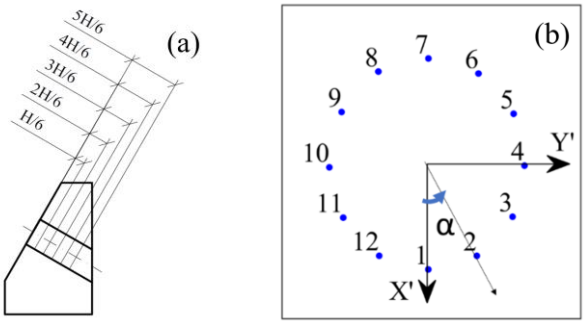

Fig. 4. Schematic representation and labeling of the position of the levels corresponding to the circle measurement (a), and the 12 nominal points acquired on each level (b).

After measurement, green parts were debinded at 470°C for 4 hours in Argon atmosphere, then heated at 5°C/min up to the isothermal sintering temperature of 1360°C for

3 hours in a vacuum furnace at the pressure of 10^{-1} mbar (HT-S1 LPC by HTS, Mozzanica BG, Italy).

Sintered samples were measured according to the same routine developed for green parts. The measurement routine was the same used for the green parts, the points acquired were theoretically located at the same fraction of the effective depth, even if not in the same identical position due to the large shrinkage occurred on sintering.

The dimensional changes of the linear dimensions and diameters were calculated according to equations (4) and (5), respectively.

$$\varepsilon_L = \frac{L_s - L_g}{L_g} \tag{4}$$

$$\varepsilon'_{\phi i} = \frac{\phi_s - \phi_g}{\phi_g} \tag{5}$$

2.2 Theoretical model

The analytical model presented hereafter aims at predicting the dimensional change on sintering and the geometrical variation of cylindrical holes. The main points of the model are here briefly recalled, description in depth can be found in [21]. As documented in scientific literature [9–11], the dimensional change on sintering is supposed to be anisotropic. Moreover, dimensional change is assumed totally dependent on the direction in the printing reference system, and independent on the sample geometry. On the basis of these assumptions, the reference system is defined according to Fig. 5. XYZ reference system is the printing reference system. X'Y'Z' reference system is related to the hole, Z' corresponds to the cylinder axis, Y' is overlapped with Y direction and θ angle defines counterclockwise rotation around Y' axis of X'Z' plane. Within X'Y'Z', the reference system in cylindrical coordinates (R,α,Z'') is identified (positive value of α corresponds to counterclockwise rotation moving from X' to Y' axis).

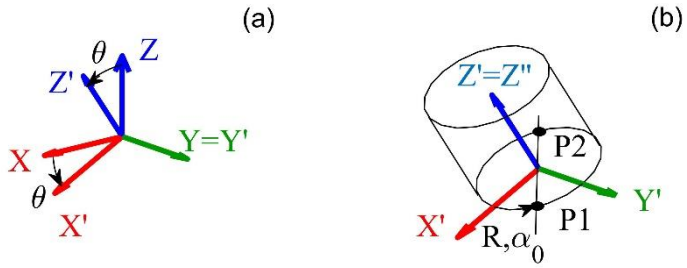

Fig. 5. Conventional reference systems of the cylindrical hole: (a) XYZ printing reference system, X'Y'Z' rotated reference system and (b) R,α,Z" cylindrical reference system.

Two diametral opposite points (P1, P2) belong to plane X'Y' and to the cylinder, therefore their radial coordinates are equal to the nominal radius of the hole (R). Assuming the angular coordinate of P1 equal to α_0, the coordinate of the diametral point P2 would

be equal to α_0 plus 180°, by definition. The two points lie on the cylindrical surface at a generic coordinate z''_0.

The coordinates of the points can be translated in the X'Y'Z' reference system by equations (6) and (7).

$$\begin{Bmatrix} x'_{P1} \\ y'_{P1} \\ z'_{P1} \end{Bmatrix} = \begin{Bmatrix} R\cos\alpha_0 \\ R\sin\alpha_0 \\ z''_0 \end{Bmatrix} \tag{6}$$

$$\begin{Bmatrix} x'_{P2} \\ y'_{P2} \\ z'_{P2} \end{Bmatrix} = \begin{Bmatrix} -R\cos\alpha_0 \\ -R\sin\alpha_0 \\ z''_0 \end{Bmatrix} \tag{7}$$

Moreover, the P1 and P2 coordinates can be expressed in the fabrication reference system (XYZ) by equation (8).

$$\begin{Bmatrix} x_{g-i} \\ y_{g-i} \\ z_{g-i} \end{Bmatrix} = \begin{bmatrix} \cos\theta_g & 0 & -\sin\theta_g \\ 0 & 1 & 0 \\ \sin\theta_g & 0 & \cos\theta_g \end{bmatrix} \begin{Bmatrix} x'_{g-i} \\ y'_{g-i} \\ z'_{g-i} \end{Bmatrix} \tag{8}$$

Where the subscript i refers to the point number and θ_g represents the angle between the cylinder axis and the building direction in the green state.

Considering the shrinkage occurring on sintering, the new coordinates of the points in the sintered state can be calculated by equation (9).

$$\begin{Bmatrix} x_{s-i} \\ y_{s-i} \\ z_{s-i} \end{Bmatrix} = \begin{bmatrix} 1+\varepsilon_x & 0 & 0 \\ 0 & 1+\varepsilon_y & 0 \\ 0 & 0 & 1+\varepsilon_z \end{bmatrix} \begin{Bmatrix} x_{g-i} \\ y_{g-i} \\ z_{g-i} \end{Bmatrix} \tag{9}$$

Where ε_x, ε_y, ε_z represent the dimensional changes along the XYZ fabrication reference system, which are defined according to equation (4). The subscripts g and s refer to the green and sintered state, respectively.

In agreement with the measurement strategy, the diameter of the hole can be estimated by the point-by-point distance. In this model, the green diameter is theoretically equivalent to the nominal value defined in the CAD file, while the sintered diameter can be evaluated by the distance of the two opposite points as by equation (10).

$$\phi'_s = \sqrt{(x'_{s-P2} - x'_{s-P1})^2 + (y'_{s-P2} - y'_{s-P1})^2 + (z'_{s-P2} - z'_{s-P1})^2} \tag{10}$$

The sintered coordinates of the points can be expressed as function of the XYZ coordinates by the rotation matrix in equation (11).

$$\begin{Bmatrix} x'_{s-i} \\ y'_{s-i} \\ z'_{s-i} \end{Bmatrix} = \begin{bmatrix} \cos\theta_s & 0 & \sin\theta_s \\ 0 & 1 & 0 \\ -\sin\theta_s & 0 & \cos\theta_s \end{bmatrix} \begin{Bmatrix} x_{s-i} \\ y_{s-i} \\ z_{s-i} \end{Bmatrix} \tag{11}$$

Where θ_s is calculated by equation (12).

$$\theta_s = \tan^{-1}\left(\frac{x_s}{z_s}\right) = \tan^{-1}\left[\tan\theta_g \frac{(\varepsilon_x+1)}{(\varepsilon_z+1)}\right] \quad (12)$$

By equations (10) and (11) the sintered diameter is derived, as defined by the coordinates in XYZ reference system, to apply the dimensional change defined in equation (9). The coordinates are then converted in the X'Y'Z' reference system by equation (8), and in the cylindrical reference system by equations (6) and (7).

Finally, the dimensional change of the hole can be predicted by equation (5), which turns to equation (13) using the terms derived above.

$$\varepsilon'_{\phi i} = \sqrt{\cos^2\alpha_0\left[(\varepsilon_x+1)^2\cos^2\theta_g + (\varepsilon_z+1)^2\sin^2\theta_g\right] + \sin^2\alpha_0\left(\varepsilon_y+1\right)^2} - 1 \quad (13)$$

In agreement with the starting hypothesis, the analytical model is independent on the cylindrical size (diameter and the depth), it depends on:

- the dimensional change along the fabrication reference system (ε_x, ε_y, ε_z);
- the orientation of the cylinder axis with respect to the building direction (θ_g);
- the angular position of the selected points on the circumference (α_0).

Summarizing, this model described the evolution of the circular section of the cylinder to an elliptical shape, as affected by the anisotropic dimensional change on sintering and by the cylinder orientation.

3 Results and discussion

All the dimensional changes on sintering of the linear dimensions, as calculated by equation (4) in all the samples, are reported in Table 3, as mean value and standard deviation.

Table 3. Average and standard deviation of the dimensional change on sintering of the linear dimensions of the five samples.

Printing direction	Average ε_L [%]	Std. Dev. ε_L [%]
X	-15.5	0.8
Y	-14.9	0.2
Z	-17.8	0.8

An almost isotropic behavior is shown in plane XY, while shrinkage is considerably higher along Z direction. The analysis of the results of linear dimensional changes is exhaustively discussed in [21].

The mean values of the linear shrinkage were used as ε_x, ε_y, ε_z input parameters in the analytical model.

Fig. 6 shows the dimensional change of the diameters of the four cylindrical holes of sample 0°. Plots from A to D in Fig. 6 refer to the holes having the nominal diameter of 3, 5, 7, 9 mm, showing the data of the experimental measurements, along with the corresponding values predicted by the analytical model. Empirical data are divided in

five groups, related to the different levels (H/6, 2H/6, 3H/6, 4H/6, 5H/6 fraction of the effective depth). Each group contains the diameter shrinkage corresponding to α angular coordinate (0°,30°,60°,90°,120°,150°).

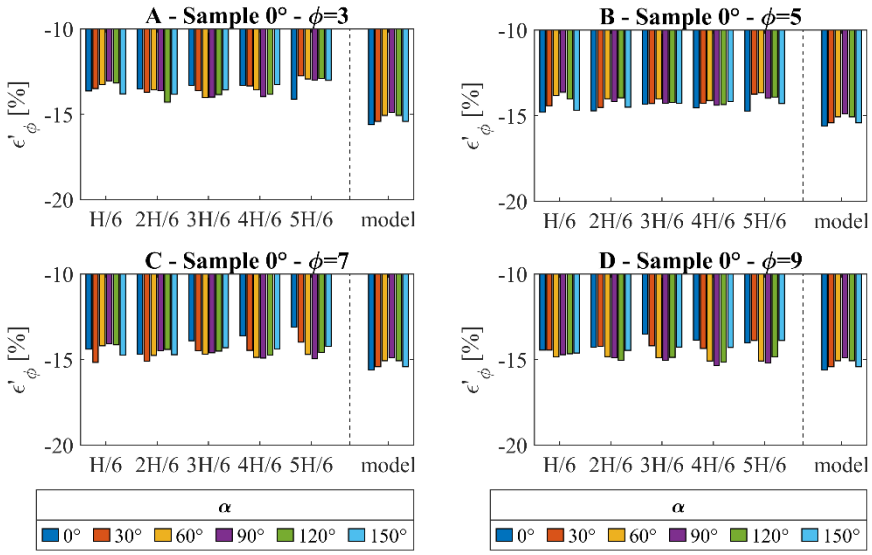

Fig. 6. Experimental and predicted dimensional change on sintering of the hole diameters evaluated at different depth and angular positions. Sample 0°: (A) hole 3 mm, (B) hole 5 mm, (C) hole 7 mm, (D) hole 9 mm.

In sample 0°, the analytical model predicts slightly lower diameter shrinkage corresponding to α angle equal to 90°, due to the slight difference between ε_y and ε_x used as input parameters. The empirical results generally show the same shrinkage at different α angles, practically unaffected by depth. Therefore, the experimental shrinkage is in line with the model prevision, concerning the influence of α angle. Nevertheless, in the biggest holes (7 and 9 mm), deeper scan levels, empirical data show an opposite trend compared to the model prevision.

Moreover, mean values of experimental data look to be affected by hole size, and larger shrinkage is observed in larger holes. The influence of hole size might be related to the amount of material surrounding the different holes: as by Fig. 1, the larger the hole, the smaller the amount of surrounding material. Considering the thermal gradient during sintering, the lower amount of material surrounding the larger holes should heat up faster than the higher amount of material surrounding the smaller holes, determining different time at the isothermal sintering temperature, and consequently different dimensional change. Future work will model and empirically study the possible temperature gradient occurring during the sintering cycle in different samples, in order to confirm this hypothesis.

Moreover, the influence of green density should be considered, and in particular the inhomogeneous green density due to irregular powder spreading in Y direction. As

reported in scientific literature, lower powder bed density determines higher dimensional variation on sintering [22]. The influence of green density will be investigated in future work, referring to different positions of samples in the working plane.

Fig. 7 shows the experimental measurements, along with the corresponding values predicted by the analytical model, for sample 90° (same grouping as in Fig. 6). The evolution of data plots from sample 0° to sample 90° is represented by the data corresponding to samples 30°, 45° and 60°, showing intermediate values according to the predicted trend. They are not shown here due to space limitations.

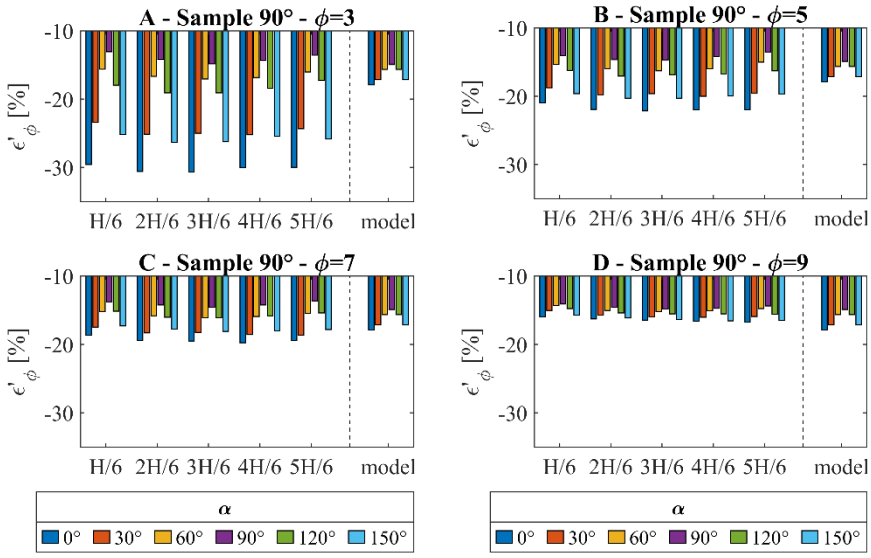

Fig. 7. Experimental and theoretical dimensional change on sintering of the hole diameters evaluated at different depth levels and angular positions. Sample 90°: (A) hole 3 mm, (B) hole 5 mm, (C) hole 7 mm, (D) hole 9 mm.

In sample 90° the trend of experimental data, as affected by α angle, fully confirms the trend predicted by the model. Shrinkage decreases on increasing α from 0° to 90°, then increases on increasing α up to 150°. Significant influence of hole size is also observed, which might be ascribed to the influence of gravity force during sintering. Considering the orientation of the sample in the working space, the mass of weakly bonded particles above the holes might have determined the distortion of the cylindrical shape of the holes. The effect is more pronounced in the smaller holes, which are subject to higher gravity force due to the higher mass of powder above the hole surface. The influence of gravity is not considered in the analytical model, and consequently the dimensional change is underestimated. Future work will consider the load induced by gravity in order to enhance the current model formulation.

4 Conclusion

This works investigated the dimensional precision of cylindrical holes produced by binder jetting process. Five samples were fabricated by AISI316L powder feedstock and sample geometry was measured before and after the sintering operation by means of a coordinate measuring machine. The experimental results were compared with the analytical solution of a model previously developed showing that:

- the analytical trend is generally confirmed. The shrinkage of diameter depends on: the anisotropic dimensional change, the angle between the cylinder axis and the building direction, and the position of the selected diametral points on the circumference.
- The difference between the measured and predicted values can be ascribed to the gravity effect and to a temperature gradient within the sample during sintering.

Further work will improve the model, also including the effect of gravity and temperature gradient, in order to develop an effective design approach for BJ. In this way, the model could be effectively adopted for compensating the CAD geometry, in order to improve the quality and standardization of BJ product.

References

1. Ziaee, M., Crane, N.B.: Binder jetting: A review of process, materials, and methods. Addit. Manuf. 28, 781–801 (2019).
2. Li, M., Du, W., Elwany, A., Pei, Z., Ma, C.: Metal Binder Jetting Additive Manufacturing: A Literature Review. J. Manuf. Sci. Eng. 142, 1–17 (2020).
3. Wiberg, A., Persson, J., Ölvander, J.: Design for additive manufacturing – a review of available design methods and software. Rapid Prototyp. J. 25, 1080–1094 (2019).
4. Kumke, M., Watschke, H., Vietor, T.: A new methodological framework for design for additive manufacturing. Virtual Phys. Prototyp. 11, 3–19 (2016).
5. Rosso, S., Savio, G., Uriati, F., Meneghello, R., Concheri, G., Rosso, S., Meneghello, R., Concheri, G., Curtarello, A., Rosso, S., Meneghello, R., Concheri, G.: Optimization approaches in design for additive manufacturing. Proc. Int. Conf. Eng. Des. ICED. 2019-Augus, 809–818 (2019).
6. Ameta, G., Lipman, R., Moylan, S., Witherell, P.: Investigating the Role of Geometric Dimensioning and Tolerancing in Additive Manufacturing. J. Mech. Des. Trans. ASME. 137, (2015).
7. Moroni, G., Petrò, S., Polini, W.: Geometrical product specification and verification in additive manufacturing. CIRP Ann. - Manuf. Technol. 66, 157–160 (2017).
8. Zago, M., Larsson, M., Cristofolini, I.: An Improved Design Method for Net-Shape Manufacturing in Powder Metallurgy. Springer International Publishing (2020).
9. Mostafaei, A., Rodriguez De Vecchis, P., Nettleship, I., Chmielus, M.: Effect of powder size distribution on densification and microstructural evolution of binder-jet 3D-printed alloy 625. Mater. Des. 162, 375–383 (2019).
10. Kumar, A., Bai, Y., Eklund, A., Williams, C.B.: Effects of Hot Isostatic Pressing on Copper Parts Fabricated via Binder Jetting. Procedia Manuf. 10, 935–944 (2017).

11. Miyanaji, H., Rahman, K.M., Da, M., Williams, C.B.: Effect of fine powder particles on quality of binder jetting parts. Addit. Manuf. 36, (2020).
12. Kafara, M., Kemnitzer, J., Westermann, H.H., Steinhilper, R.: Influence of Binder Quantity on Dimensional Accuracy and Resilience in 3D-Printing. Procedia Manuf. 21, 638–646 (2018).
13. Islam, M.N., Sacks, S.: An experimental investigation into the dimensional error of powder-binder three-dimensional printing. Int. J. Adv. Manuf. Technol. 82, 1371–1380 (2016).
14. Ollison, T., Berisso, K.: Three-dimensional printing build variables that impact cylindricity. J. Ind. Technol. 26, 1–10 (2010).
15. Baselli, S., Torresani, E., Zago, M., Amirabdollahian, S., Cristofolini, I., Molinari, A.: Sintering shrinkage of uniaxial cold compacted iron: influence of the microstructure on the anisothermal and isothermal shrinkage of uniaxial cold-compacted iron. Powder Metall. 61, 276–284 (2018).
16. Zago, M., Cristofolini, I., Molinari, A.: New interpretation for the origin of the anisotropic sintering shrinkage of AISI 316L rings based on the anisotropic stress field occurred on uniaxial cold compaction. Powder Metall. 62, 115–123 (2019).
17. Cristofolini, I., Molinari, A., Zago, M., Amirabdollahian, S., Coube, O., Dougan, M.J., Larsson, M., Schneider, M., Valler, P., Voglhuber, J., Wimbert, L.: Design for Powder Metallurgy: Predicting Anisotropic Dimensional Change on Sintering of Real Parts. Int. J. Precis. Eng. Manuf. 20, 619–630 (2019).
18. Mirzababaei, S., Pasebani, S.: A review on binder jet additive manufacturing of 316L stainless steel. J. Manuf. Mater. Process. 3, 8–12 (2019).
19. Vitolo, F., Martorelli, M., Gerbino, S., Patalano, S., Lanzotti, A.: Controlling form errors in 3D printed models associated to size and position on the working plane. Int. J. Interact. Des. Manuf. 12, 969–977 (2018).
20. ISO, I.S.O.: 10360-2: 2009—Geometrical Product Specifications (GPS)—Acceptance and Reverification Tests for Coordinate Measuring Machines (CMM)—Part 2: CMMs Used for Measuring Linear Dimensions. Int. Organ. Stand. Gevena, Switz. (2009).
21. Zago, M., Lecis, N.F.M., Vedani, M., Cristofolini, I.: Dimensional and geometrical precision of parts produced by Binder Jetting process as affected by the anisotropic shrinkage on sintering. Addit. Manuf. 43 (2021) 102007.
22. Do, T., Shin, C.S., Stetsko, D., Vanconant, G., Vartanian, A., Pei, S., Kwon, P.: Improving Structural Integrity with Boron - Based Additives for 3D printed 420 Stainless Steel. Procedia Manuf. 1, 263–272 (2015).